Physically Tenable Analysis and Control of Scattering from Reconfigurable Intelligent Surfaces

Botond Tamás Csathó, *Graduate Student Member, IEEE, Member, HTE,* and Bálint Péter Horváth

***Abstract*—Reconfigurable intelligent surface is a promising concept within the scope of smart radio environment, which is a key enabler of the future wireless networks. Efficient numerical modeling of such devices constitutes a fundamental and actively pursued research challenge. This study numerically analyzes the reflection properties of a particular reconfigurable intelligent surface with the aid of computational electromagnetics. A key advantage of utilizing full-wave simulations is that they capture all the physical phenomena within the structure, thus providing a physically stenable analysis method. An essential aspect of RIS modeling is the configuration pattern design of the surfaces. A standard objective function of the pattern design is the amount of energy reradiated toward the target direction. The utilization of full-wave simulations limits the applicable optimization methods. In this article, an intuition-based pattern search method is presented to design RIS configurations, with the radiation pattern of the RIS structure in free space as the objective function. The suggested method first identifies a set of configuration values, then exhaustively searches through their combinations, seeking for the highest anomalously reflected power. The first presented result is the demonstration of creating anomalous reflections, with the dominant reflection being electrically tunable. The second contribution is the aforementioned pattern search method, which enables the reradiation of the incident energy for numerous anomalous directions. The average scattering parameter amplitude for the scenario is 0.78. Finally, we also demonstrate the effect of the structure being finite in size. We conclude that the dominant radiation directions coincide with the modes of the infinite periodic counterpart.**

***Index Terms*—Reconfigurable Intelligent Surface (RIS), Intelligent Reflecting Surfaces (IRS), configurable MeTaSurfaces (MTS), periodic structures, full-wave simulation**

I. INTRODUCTION

THE smart radio environment (SRE) is a paradigm that has recently emerged to meet the unprecedented requirements of future wireless networks such as sixth generation (6G) [1]. The fundamental idea of SRE is to jointly optimize the wireless channel and the communicating endpoints [1]. The idea of reconfigurable intelligent surfaces (RISs) is a chief concept within the scope of SRE [2]. An RIS is a surface designed to configurably modify the scattered electromagnetic (EM) field [2].

An RIS consists of numerous elements (unit cells) whose EM properties can be electronically adjusted, for example, with tunable varactor diodes [3], switchable positive-intrinsic-negative diodes [4] or liquid crystal technology [5]. An RIS can be designed based on the well-established concept of reflectarrays or metasurface (MTS) technology [6]. The latter is superior due to the available EM field transformations [6], and utilized, e.g., to improve antenna structures [6]–[8]. It is important to note that RISs are primarily envisioned as nearly passive devices, meaning only their configuration requires energy. Numerous visions exist for scenarios where an RIS deployment is beneficial [9]. These include communicating with a user in blockage, creating additional signal paths, increasing the channel rank, and suppressing interference.

The interaction between the impinging EM field and the RIS can be described with macroscopic or microscopic models. Macroscopic models omit the particular structure of the unit cells and instead use some macroscopic parameters to account for the effect of the surface. Some frequently used macroscopic models are reviewed in [2], [10]. Numerous macroscopic models are employed to design control algorithms and large-scale performance evaluation. Some make simplifications that mask fundamental physical behavior, such as the interaction between neighboring RIS elements, e.g., [11]. In contrast, some macroscopic models are physically tenable; these are often used for the design of metasurfaces; one such model is the generalized sheet-transition condition [7]. Macroscopic models can also be included in ray-tracing simulators suitable for large-scale performance analysis [10].

On the contrary, microscopic models consider the physical implementation of unit cells. Conventionally, this requires full-wave numerical simulation of the structure. Therefore, these models are physically tenable and can capture fundamental phenomena. Full-wave simulations are commonly employed in the design phase [12], and to retrieve macroscopic parameters or validate macroscopic models [7]. Since the full-wave simulation of the complete propagating environment in 3D is resource-demanding, they are not feasible to conduct a large-scale performance evaluation. To circumvent the resource-demand issue, one can improve the efficiency of the numerical models [13]–[15], alternatively, the amalgamation of microscopic and macroscopic models can be employed [16]. The advantage of microscopic models lies in their applicability to almost any unit cell structure, particularly given the computational power available today. Hence, it is possible to analyze cases when homogenization-based macroscopic models are not suitable due to the physical dimensions of the unit cell relative to the wavelength.

Designing RIS control patterns constitutes a fundamental goal of RIS modeling. The choice of the RIS model is interconnected with the pattern design or beamforming methods. With simple macroscopic models, it is possible to optimize the RIS for a particular statistical channel realization [11], [17], [18]. With physically tenable macroscopic models, the typical goal is to tune the reflection pattern of the RIS to

The authors are with the Department of Broadband Infocommunications and Electromagnetic Theory, Budapest University of Technology and Economics, Budapest, Hungary. (E-mail: csatho.botond@edu.bme.hu, horvath.balint@vik.bme.hu)

DOI: 10.36244/ICJ.2025.1.5

achieve the desired pattern while omitting the effect of the environment [6], [12], [19]. From this perspective, microscopic models are similar; i.e., often the reflection pattern of the surface is optimized without considering the environment [13], [14]. In our work, a full-wave simulation-based approach is applied for RIS modeling, considering the size of the analyzed structure relative to the wavelength. An issue of significant importance with full-wave simulation-based RIS pattern design is that as the number of continuous control parameters increases, the optimization problem becomes more computationally demanding. The present article provides an intuition-based solution for this challenge. A more detailed comparison of different RIS pattern design methods is provided after discussing our contribution in Tab. III.

The considered design is based on a prototype described in the literature [3]. We assume that unit cells are configured periodically; consequently, only one period (so-called super-cell) is analyzed. As a first result, we present fundamental effects related to plane wave (PW) scattering from an RIS. Our main contribution is a method to generate RIS configuration patterns to achieve anomalous reflection. The presented method can be utilized to determine advantageous patterns if an RIS design is provided. We demonstrate that it is possible to direct power into configurable reflection directions. Our observations are consistent with the capabilities of antenna arrays and reflectarray technology; namely, by proper phase pattern design, it is possible to create anomalous reflection, i.e., turn the main beam in the desired direction [12]. Such anomalous reflections can be achieved, e.g., with phase-gradient metasurfaces designed based on the generalized Snell's law [12]. In a real-life RIS deployment, one should consider the limited physical size of an RIS. Therefore, as a last result, we compare the scattering properties of a finite-size RIS with the ones of an infinite periodic structure.

The remainder of the manuscript is organized as follows. Section II describes the core concept of EM field scattering from planar periodic structures. Subsequently, the utilized full-wave solver and the analyzed design are introduced in Sec. III. The results obtained from full-wave simulations and the description of the suggested pattern search method are presented in Sec. IV. Finally, conclusions are drawn in Sec. V.

The following mathematical notation is used throughout this paper. $\|\cdot\|$ denotes the 2-norm, $|\cdot|$ and $\arg(\cdot)$ are the absolute value and argument of a complex scalar, respectively. $\mathbb{Z}$, $\mathbb{R}$, $\mathbb{C}$ are sets of integer, real, and complex numbers, respectively.

II. Reflection from Periodic Structures

Let us start with an overview of the EM scattering from periodic structures, which is vital for analyzing the simulation results. We consider an infinite planar periodic structure consisting of rectangular lattices located at $z = 0$ with a PW incident on the surface. The period sizes and the angles describing the wave vectors of the incident and reflected PW, namely θ_i, ϕ_i, θ_r, and ϕ_r are shown in Fig. 1. Subscripts i and r indicate incident and reflected, respectively. The wave vectors

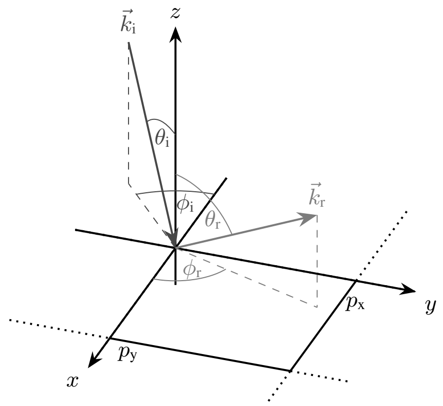

Fig. 1. Incident ($\vec{k}_\mathrm{i}$) and reflected ($\vec{k}_\mathrm{r}$) plane waves and and periodicity (p_x, p_y) of the structure

can be computed as

$$\begin{aligned}\left\|\vec{k}_\nu\right\| &= k_\nu = \frac{2\pi}{\lambda} = \frac{2\pi f}{c} = 2\pi f\sqrt{\mu\varepsilon},\\ \vec{k}_\nu &= k_{\nu,\mathrm{x}}\hat{x} + k_{\nu,\mathrm{y}}\hat{y} + k_{\nu,\mathrm{z}}\hat{z},\\ &\text{with } \nu \in \{\mathrm{i},\mathrm{r}\}\,,\end{aligned} \tag{1}$$

where λ is the wavelength, f is the frequency, c is the speed of light in the medium, μ and ε are the permeability and permittivity of the medium in the $z \geq 0$ region, respectively. Furthermore, $\hat{x}$, $\hat{y}$, and $\hat{z}$ are the unit vectors in the X-, Y-, and Z-axes, respectively.

Applying the Floquet-Bloch theory, it can be shown that the scattered EM field of a periodic structure can be expressed as a linear combination of particular PW components [20]. It can be derived that the wave vector of these components is determine by the periodicity of the structure. According to Bhattacharyya [20], in the case of a rectangular grid, such as the one in Fig. 1, these wave vectors are

$$\begin{aligned}k_{\mathrm{r,x},m} &= k_\mathrm{i,x} + \frac{2\pi m}{p_\mathrm{x}},\\ k_{\mathrm{r,y},n} &= k_\mathrm{i,y} + \frac{2\pi n}{p_\mathrm{y}},\\ &\{n, m\} \in \mathbb{Z},\end{aligned} \tag{2}$$

where p_x and p_y are the length of the period of the structure along the X-axis and Y-axis, respectively, or in other terms, the size of the super-cell. Let us note here that equation (2) can be extended for general grids [20]. An m, n pair is also referred to as a mode. For each mode

$$k_\mathrm{i}^2 = k_\mathrm{r}^2 = k_{\mathrm{r},m,n}^2 = k_{\mathrm{r,x},m}^2 + k_{\mathrm{r,y},n}^2 + k_{\mathrm{r,z},m,n}^2 \tag{3}$$

must hold, which also defines $k_{\mathrm{r,z},m,n}$. Consequently,

$$\begin{aligned}k_{\mathrm{r,x},m}^2 + k_{\mathrm{r,y},n}^2 < k_\mathrm{r}^2 &\iff \text{propagating mode},\\ k_{\mathrm{r,x},m}^2 + k_{\mathrm{r,y},n}^2 > k_\mathrm{r}^2 &\iff \text{evanescent mode}.\end{aligned} \tag{4}$$

Only propagating modes, i.e., when $k_{\mathrm{r,z},m,n} \in \mathbb{R}$ and $k_{\mathrm{r,z},m,n} > 0$ can deliver power to the far-field. The energy propagating in each mode depends on the boundary conditions (BCs) imposed by the structure.

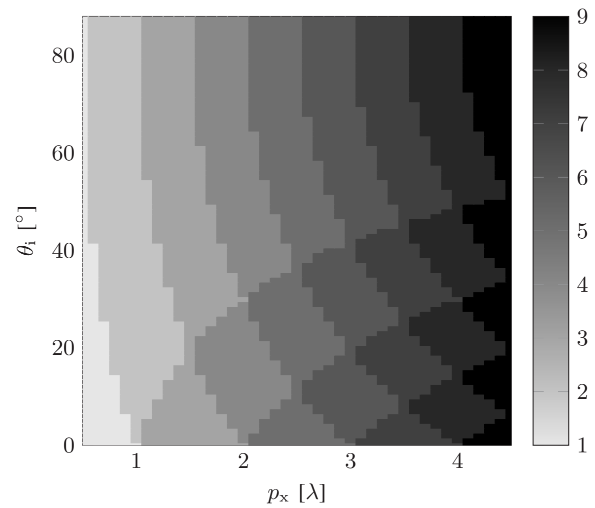

Fig. 2. Demonstrating the effect of varying the period size and incident angle on the number of propagating modes, assuming $\phi_\mathrm{i} = 0\,°$, $p_\mathrm{y} = \lambda$

The number of propagating modes can be determined using (1), (2), (3), and (4). Figure 2 demonstrates the number of propagating modes for varying periodicity and incident angles. One can observe that as the period size increases with respect to the wavelength, the number of propagating modes also increases. Furthermore, the incident angle also affects the possible number of modes.

In conclusion, the period size and the angle of incidence govern the propagating modes By changing the structure, e.g., by modifying some geometrical parameter or tuning an electrically configurable component, it is possible to adjust the power corresponding to each propagating mode, as presented in Sec. IV.

III. Numerical Analysis

A. Simulation Environment

A commercial full-wave EM simulation software[1] is used to study scattering from an RIS in a physically consistent manner. The software solves Maxwell's equations with the finite element method. We assume that the RIS is configured periodically. Therefore, it can be treated as an infinite periodic structure, providing that the effect of the edges is neglected. Accordingly, analyzing only one period, i.e., a super-cell, is sufficient. PW excitation is used for the analysis, which does not restrict generality since an arbitrary EM field can be decomposed into the appropriately weighted sum of PWs with spatial Fourier transform [21]. HFSS can determine the possible propagating modes based on the size of the super-cell and the direction of the impinging PW. For each mode, it defines two ports, one for transverse electric (TE) and one for transverse magnetic (TM) polarization[2].

[1] Ansys® Academic Research High-Frequency Structure Simulator (HFSS) Release 2021 R2

TABLE I
NUMERICAL DATA RELATED TO THE RIS STRUCTURE DEPICTED IN FIG. 3

Variable	Value	Variable	Value
p_x	31.4 mm	l_4	0.6 mm
p_y	22.6 mm	l_5	2.9 mm
l_1	20.3 mm	l_6	4.3 mm
l_2	4 mm	l_7	0.6 mm
l_3	8.3 mm	t_1	3 mm
ε_1	$2.65\varepsilon_0$	$\tan\delta_1$	0.005
μ_1	μ_0		

We are interested in the scattering parameters (S-parameters) of the super-cell. These are initially defined as the ratio of incident and reflected voltages in an N-port network. HFSS can provide these metrics in terms of EM fields. According to the definition of S-parameters,

$$S_{j;k} = \left.\frac{\Psi_{\mathrm{r},j}}{\Psi_{\mathrm{i},k}}\right|_{\Psi_{\mathrm{i},k}=0 \text{ if } l\neq k}, \; j,k,l = 1,\ldots,\mathrm{N}, \tag{5}$$

where $S_{j;k} \in \mathbb{C}$, N is the number of ports defined by HFSS, and $\Psi_{\mathrm{r},j}$, $\Psi_{\mathrm{i},k}$ are unitless complex amplitudes of the reflected and incident fields corresponding to the j^{th} and k^{th} port, respectively [23]. Therefore,

$$\sum_{j=1}^{\mathrm{N}} \left|S_{j;k}\right|^2 \leq 1, \; \forall k, \tag{6}$$

must hold if the structure is passive because of the principle of conservation of energy. One needs to verify that the simulation results satisfy (6), since this is a straightforward indicator of a physically meaningful model.

As an example of the utilized notation, $S_{0,0,\mathrm{TE};1,0,\mathrm{TM}}$ is the scattering parameter corresponding to the $m = 0, n = 0$ mode in TE polarization, if the excitation is given in the $m = 1, n = 0$ mode with TM polarization.

B. Analyzed Unit Cell

Let us now introduce the studied RIS design. The unit cell arrangement is based on a manufactured and measured prototype [3]. We tune the original structure to operate around $f = 4.7\,\mathrm{GHz}$ (5G New Radio Frequency Range 1 n79 band). The sketch of the HFSS model is shown in Fig. 3, while the parameter values are summarized in Tab. I, where ε_0 and μ_0 denote the permittivity and the permeability of the vacuum, respectively. In the original design, there is a second substrate layer for the biasing lines, which is omitted in the HFSS model to save resources. Therefore, the biasing lines are connected to the ground.

In the HFSS model, periodicity is incorporated using `Lattice Pair` type BCs. A `Floquet Port` is the source of the PW excitation. The varactor diodes are modeled with `Lumped RLC` BCs, with zero resistance and inductance. The

[2] Let us note that the EM scattering from a boundary is usually described with TE and TM polarized components. These components are orthogonal to each other. Moreover, an arbitrary PW can be decomposed into TE and TM polarized components with respect to a plane [22].

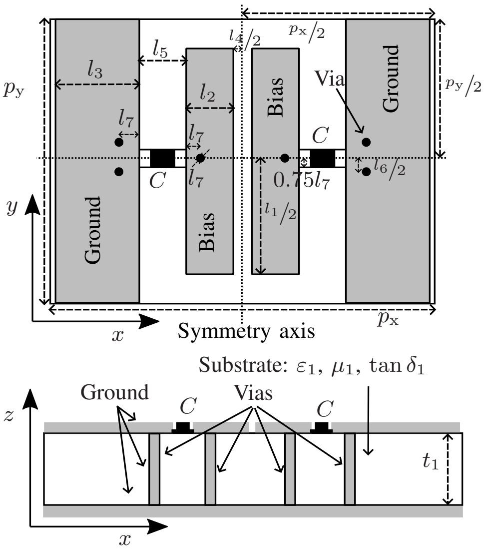

Fig. 3. Analyzed RIS structure. Parameter values are shown in Tab. I. $\tan\delta$ denotes the dielectric loss tangent.

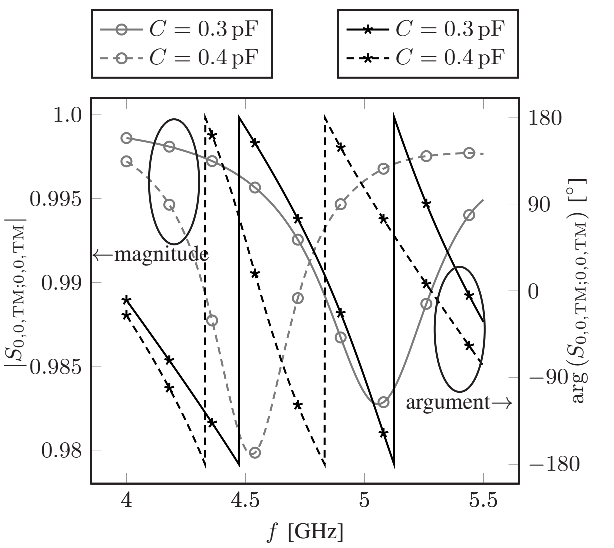

Fig. 4. Magnitude and argument of the complex-valued scattering parameter of a single unit cell $\theta_\mathrm{i} = \phi_\mathrm{i} = 0\,°$

capacitance (C) values are the control parameters of the RIS and equal within a unit cell. All chopper parts are considered with `Perfect E` BCs. The substrate is modeled as a user-defined dielectric, and there is a vacuum above the RIS.

The scattering parameters of the model are shown in Fig. 4. The curves are obtained with `Interpolating HFSS Frequency Sweep` based on the solutions corresponding to 10 different frequencies, with a mesh generated at $5.5\,\mathrm{GHz}$.

IV. RESULTS AND DISCUSSION

A. Analyzing Scattering Properties

Having introduced the design, the first presented result is the angular behavior of a single unit cell. Assuming that the excitation is applied in TM mode, the scattering parameters are shown in Fig. 5. The results for the TE polarized excitation are very similar; thus, we omit the corresponding results for brevity. The S-parameters can exhibit extreme deviations for varying incident angles. Furthermore, one can observe that C also affects reflection properties. In the presented case, it can turn the mode conversion from TM to TE on and off.

In the case of a single unit cell, there is only one propagating mode with the considered physical parameters. Next, we add a second unit cell along the X-axes. Consequently, two other propagating modes appear due to the nature of periodic structures, as described in Sec. II. These new propagating modes can reflect power anomalously. Figure 6 presents the scattering parameters for varying incidence angle and control parameters. On the one hand, it is apparent that by varying the control parameters, the scattering parameter of a mode can be tuned. On the other hand, one can see that power can be directed in multiple directions simultaneously, leading to reradiation toward unintended directions. Some of these signal components might cause interference. Furthermore, results suggest that interference can be mitigated by appropriately designing the control patterns.

Designing anomalously reflecting metasurfaces with perfect reflection is also described in the literature; see e.g. [12], [19]. It is noteworthy that it has also been shown that perfect anomalous reflection can be achieved, although with polarization conversion [24]. Therefore, this observation underpins the correctness of the analysis approach used in this article. It is important to emphasize that the full-wave simulation based analysis can be applied also to structures where homogenization is not feasible due to their physical dimensions relative to the wavelength. A comparison of different analysis methods is provided in Tab. III. The chosen approach also influences the potential pattern design or beamforming strategy. In the next subsection, we outline one possibility for maintaining manageable computational complexity when applying full-wave simulation.

B. RIS Pattern Search Method

In a nutshell, the fundamental difficulty arises from the number of continuous control parameters. Here, we propose an intuition-based solution to this problem by discretizing the continuous control parameters. The suggested pattern search method starts with identifying a capacitance set from which the C values are chosen. Then, we exhaustively search for optimal control parameter patterns of super-cells consisting of multiple unit cells.

To identify the set of capacitances, a single unit cell is considered. Assuming perpendicular incidence, C is tuned with the `Optimizer` available in the `Optimetrics` of HFSS to achieve a particular phase of the S-parameters at the carrier frequency ($f = 4.7\,\mathrm{GHz}$). The results are summarized in Tab. II. The authors of [3] also used a similar

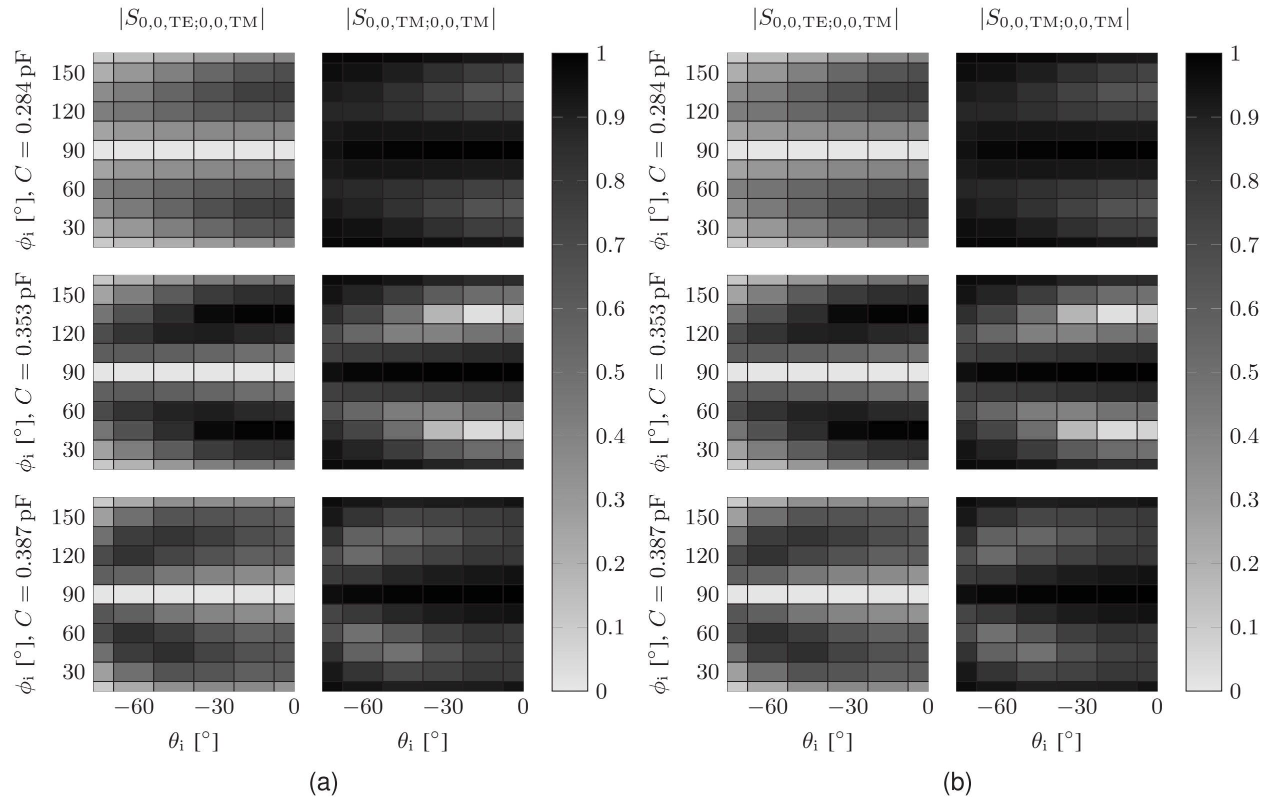

Fig. 5. Angular dependence of scattering parameters for a single unit cell, $f = 4.7$ GHz. (a) and (b) represents the magnitude and the phase of the S-parameters, respectively.

approach to determine the set of possible bias voltage values for each varactor diode. Subsequently, we choose control parameter values from Tab. II. For period sizes up to three unit cells, we use the capacitance values corresponding to $90°, 45°, 0°, -45°, -90°, -180°$. Whereas for larger period sizes, the values corresponding to $90°, 0°, -90°$ are employed to render the number of permutations manageable. Then, an exhaustive search is carried out for gradually increasing super-cell sizes. Simulations are evaluated for every possible control parameter permutation for each super-cell. First, we generate all possible permutations of the control parameters. Some permutations are then removed based on two aspects of the periodic BC. *(i)* the patterns which are cyclic shifts of an already evaluated one are ignored; e.g., only one of $C_1 = 0.284\,\mathrm{pF}, C_2 = 0.353\,\mathrm{pF}$ and $C_1 = 0.353\,\mathrm{pF}, C_2 = 0.284\,\mathrm{pF}$ is considered, where C_1 and C_2 denote the control parameter values of the two unit cells of the super-cell. *(ii)* a pattern is omitted if its periodicity is smaller than the size of the super-cell; e.g., $C_1 = C_2 = 0.353\,\mathrm{pF}$ is ignored for evaluating super-cells consisting of two unit cells since it is already considered for the case of a single unit cell. To enhance traceability, ϕ_i is set to $0\,°$. However, we would like to stress that the S-parameters depend on ϕ_i. An example of the obtained curves is shown in Fig. 6. As one can observe, the applied control pattern influences the amount of power directed into each mode.

TABLE II
CONTROL PARAMETER VALUES, $\theta_\mathrm{I} = \phi_\mathrm{I} = 0\,°$, $f = 4.7$ GHz

C [pF]	$\approx \arg\left(S_{0,0,\mathrm{TM};0,0,\mathrm{TM}}\right)$ [°]
0.051	135
0.284	90
0.330	45
0.353	0
0.374	−45
0.387	−90
0.423	−135
0.500	−180

The mode indices can be converted into reflected angles, given the incident angle and periodicity based on (1), (2), (3), and (4). Assuming $\phi_\mathrm{i} = 0\,°$, and $-90\,° < \theta_\mathrm{i} < 90\,°$, it follows that for propagating modes

$$\begin{aligned} k_{\mathrm{i,x}} &= k_0 \sin\theta_\mathrm{i}, k_{\mathrm{i,y}} = 0, \\ k_{\mathrm{r,x},m} &= k_{\mathrm{i,x}} + \frac{2\pi m}{p_\mathrm{x}}, \{m\} \in \mathbb{Z}, \\ \theta_\mathrm{r} &= \arcsin\frac{k_{\mathrm{r,x},m}}{k_0}. \end{aligned} \tag{7}$$

Let us note that (7) holds if modes corresponding to $n \neq 0$ are evanescent, which is valid for the considered period size, namely $p_\mathrm{y} = 22.6\,\mathrm{mm} \approx 0.35\,\lambda$.

The mode indices are converted to reflection angles using (7). Subsequently, we made a collection of possible θ_i-θ_r pairs.

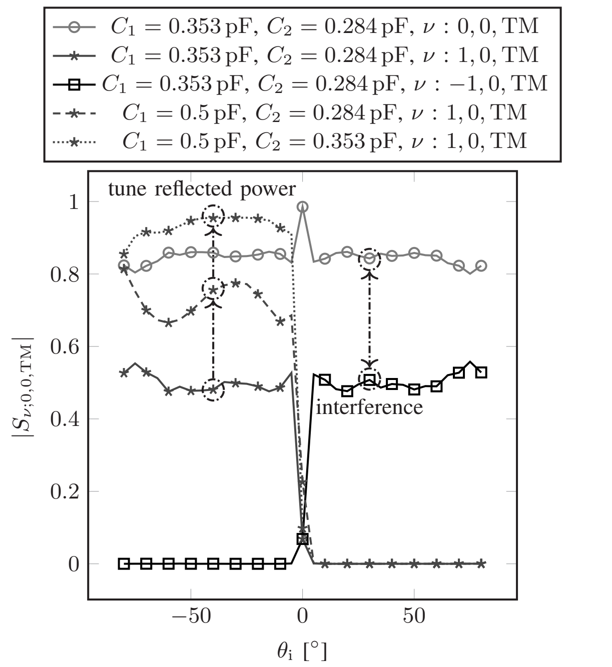

Fig. 6. Scattering parameters for a two unit cell size super-cell, $\phi_\mathrm{i} = 0\,°$, $f = 4.7\,\mathrm{GHz}$. TE modes are omitted due to their low power for these particular cases. Examples of power adjustment and interference is marked.

If a pattern for a θ_i-θ_r pair provides higher reflected power than the corresponding pattern in the database, the new pattern and its associated S-parameter are stored instead in the database for that particular θ_i-θ_r pair. Figure 7 illustrates the collection obtained for gradually increasing the maximum period size. The average of the amplitude of the scattering parameters, considering the largest period size is 0.78. Therefore, one can conclude that increasing the super-cell size makes it possible to direct power in more directions. Furthermore, one can tune the direction of reflection by choosing different patterns from the precalculated database. Continuing this approach for larger super-cell sizes and more control parameter values provides more options, presumably with higher reflection coefficients. Table III compares this approach with other strategies described in the literature relying on different RIS models. In conclusion, this intuition-based method is physically tenable and can handle structures where homogenization is not feasible, requiring higher but manageable complexity.

C. Effect of Finite Size

In practice, an RIS structure is finite in size. In turn, we also investigate the effect of this condition, which is studied analytically in the literature, see, e.g. [19]. To demonstrate this effect, we consider a six unit cell large structure, remove the periodic boundary conditions, and terminate the simulation domain with a perfectly matched layer. For the sake of simplicity, we select control parameters with a two unit cell period size and repeat it three times to obtain the patterns of the six unit cell large RIS. In this way, the pattern still has some periodicity, supporting the comparison with the periodic case. Afterward, the directivity [23] as the function of the reflection angle ($D(\phi_\mathrm{r})$) is evaluated in the far-field.

Since a pattern consisting of two unit cells is repeated three times to obtain a six unit cell large structure, the reflection angles corresponding to each propagating mode are computed using (7) with $p_\mathrm{x} = 62.8\,\mathrm{mm}$, i.e., the size of two unit cells of the considered design along the X-axis, see Tab. I.

To compare the results of the infinite periodic structure with their finite counterparts, the directions corresponding to the propagating modes are plotted on the $D(\phi_\mathrm{r})$ curves; see Fig. 8. For large incidence angles (θ_i), there is a notable difference between the peaks of $D(\phi_\mathrm{r})$ and the directions of the propagating modes. However, as the angle of incidence decreases, the peaks approach the directions indicated by the propagating modes. The effect of varying the control parameters is also apparent. For uniform configurations, specular reflection dominates, i.e., the $0, 0$ mode. By appropriately changing the control pattern, anomalous reflections can be achieved; see the curves corresponding to $C_1 = 0.353\,\mathrm{pF}, C_2 = 0.5\,\mathrm{pF}$ and $C_1 = 0.5\,\mathrm{pF}, C_2 = 0.353\,\mathrm{pF}$ in Fig. 8. From the authors' perspective, these results indicate that it might be beneficial to consider infinite periodic structures at the pattern design phase because it simplifies the simulation. However, one should keep in mind that for a finite-size RIS the directions corresponding to the highest radiated power might deviate from the directions in the case of an infinite periodic structure.

V. Conclusion

We briefly introduce periodic structures essential for understanding the full-wave simulation results. Then, a comprehensive numerical analysis of the scattering from the utilized RIS design is presented. The analyzed structure is on a length scale, where homogenization-based modeling is not feasible. Full-wave simulations were employed to address this issue. Our main contribution is the approach that enables the identification of RIS configuration patterns creating anomalous reflection. In particular, the described method is physically meaningful due to the utilization of computational electromagnetics. With this approach, a database of configuration patterns can be obtained, each targeting a different reflection direction and a low level of parasitic reflection. An RIS control algorithm can be designed based on such a database, which chooses the best control pattern from the control patterns constructed offline. The primary limitation of this approach is its run-time and computation resource demand. As the number of control parameters grows, the number of simulations also increases. This issue can be partially addressed through parallelization, which is available in most commercial full-wave solvers. Another potential solution is to limit the period size of the pattern and repeat it along the surface. We also present the following effects described in the literature. First, reflection in unintended directions might lead to implementation challenges. Second, because of the finite size of the RIS, scattering from the surface can not be described with the superposition of Floquet modes; instead, for example, the directivity can be utilized. It is noteworthy that in the evaluated scenario, the directivity peaks divert from the directions corresponding

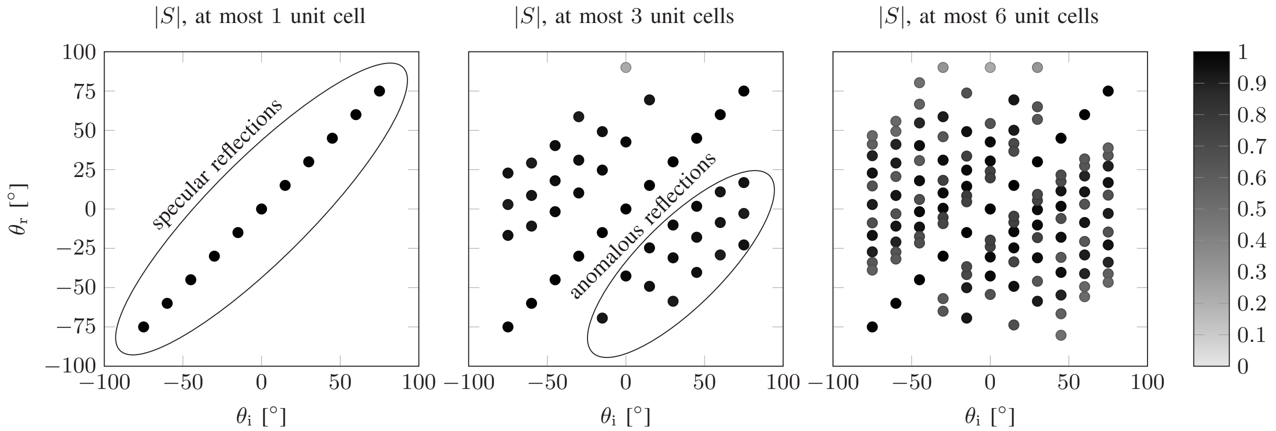

Fig. 7. Possible reflection directions, $\phi_{\mathrm{i}} = 0\,°$, $f = 4.7\,\mathrm{GHz}$. The excitation is TM polarized. For the results, both reflected polarizations are considered.

TABLE III
COMPARING DIFFERENT RIS MODELING AND CORRESPONDING PATTERN DESIGN APPROACHES

Ref.	Methodology	Objective	Strength	Limitation
[11], [17]	The effect of scatterers is represented by complex numbers in a diagonal or dense matrix.	Typically, the goal is to maximize the throughput of the RIS-aided link.	This model integrates well into the stochastic models of unstructured rich scattering channels; thus, it is possible to consider the environment.	Such models often mask fundamental physical mechanisms.
[18]	The interaction of the RIS elements is accounted for using a multiport network theory model.	Synthesize a desired radiation pattern by tuning the impedance values describing the RIS elements.	It could be more accurate than [11] and it is still suitable for numerous evaluations, e.g., in optimization loops.	Network theory-based equivalent models are usually valid for a certain frequency range.
[6], [12], [19]	The RIS is replaced by an equivalent homogenized boundary condition.	Synthesize a desired radiation pattern by creating a spatially varying boundary condition.	This approach captures all the essential physical phenomena, provided that the conditions required for homogenization are fulfilled.	It can be cumbersome to establish the correspondence of the physical structure and the parameters of the homogenized BC.
[13], [14]	An integral equation-based approach is applied. The metallic pattern is considered with an impedance type BC.	Tune the impedance BC to achieve a target radiation pattern.	It accurately captures the interaction between each part of the RIS.	Adding other structures to the model, such as vias or circuit components might be challenging.
This work	Full-wave simulation is applied.	Design a control pattern dictionary for the angle of incident and reflection pairs.	This approach captures all the physical phenomena and can be applied to structures being large relative to the wavelength.	The simulation demands more computational resources than other approaches.

to the propagating modes of the infinite case only for large incidence angles. Therefore, the results of the periodic case can serve as a reliable guideline when designing RIS patterns. Building on the presented results, a possible future direction is to apply sensitivity analysis to identify the capacitance set from which the patterns are constructed.

REFERENCES

[1] M. D. Renzo, A. Zappone, M. Debbah, M.-S. Alouini, C. Yuen, J. de Rosny, and S. Tretyakov, "Smart radio environments empowered by reconfigurable intelligent surfaces: How it works, state of research, and the road ahead," *IEEE Journal on Selected Areas in Communications*, vol. 38, no. 11, pp. 2450–2525, Nov. 2020, DOI: 10.1109/JSCA.2020.3007211.

[2] M. D. Renzo, F. H. Danufane, and S. Tretyakov, "Communication models for reconfigurable intelligent surfaces: From surface electromagnetics to wireless networks optimization," *Proceedings of the IEEE*, vol. 110, no. 9, pp. 1164–1209, Sep. 2022, DOI: 10.1109/JPROC.2022.3195536.

[3] X. Pei, H. Yin, L. Tan, L. Cao, Z. Li, K. Wang, K. Zhang, and E. Björnson, "RIS-aided wireless communications: Prototyping, adaptive beamforming, and indoor/outdoor field trials," *IEEE Transactions on Communications*, vol. 69, no. 12, pp. 8627–8640, Dec. 2021, DOI: 10.1109/TCOMM.2021.3116151.

[4] L. Dai, B. Wang, M. Wang, X. Yang, J. Tan, S. Bi, S. Xu, F. Yang, Z. Chen, M. D. Renzo, C.-B. Chae, and L. Hanzo, "Reconfigurable intelligent surface-based wireless communications: Antenna design, prototyping, and experimental results," *IEEE Access*, vol. 8, pp. 45 913–45 923, Mar. 2020, DOI: 10.1109/ACCESS.2020.2977772.

[5] O. H. Karabey, A. Gaebler, S. Strunck, and R. Jakoby, "A 2-D electronically steered phased-array antenna with 2×2 elements in LC display technology," *IEEE Transactions on Microwave Theory and Techniques*, vol. 60, no. 5, pp. 1297–1306, May 2012, DOI: 10.1109/TMTT.2012.2187919.

[6] E. Martini and S. Maci, "Theory, analysis, and design of metasurfaces for smart radio environments," *Proceedings of the IEEE*, vol. 110, no. 9, pp. 1227–1243, Sep. 2022, DOI: 10.1109/JPROC.2022.3171921.

[7] C. L. Holloway, E. F. Kuester, J. A. Gordon, J. O'Hara, J. Booth, and D. R. Smith, "An overview of the theory and applications of metasurfaces: The two-dimensional equivalents of metamaterials," *IEEE Antennas and Propagation Magazine*, vol. 54, no. 2, pp. 10–35, Apr. 2012, DOI: 10.1109/MAP.2012.6230714.

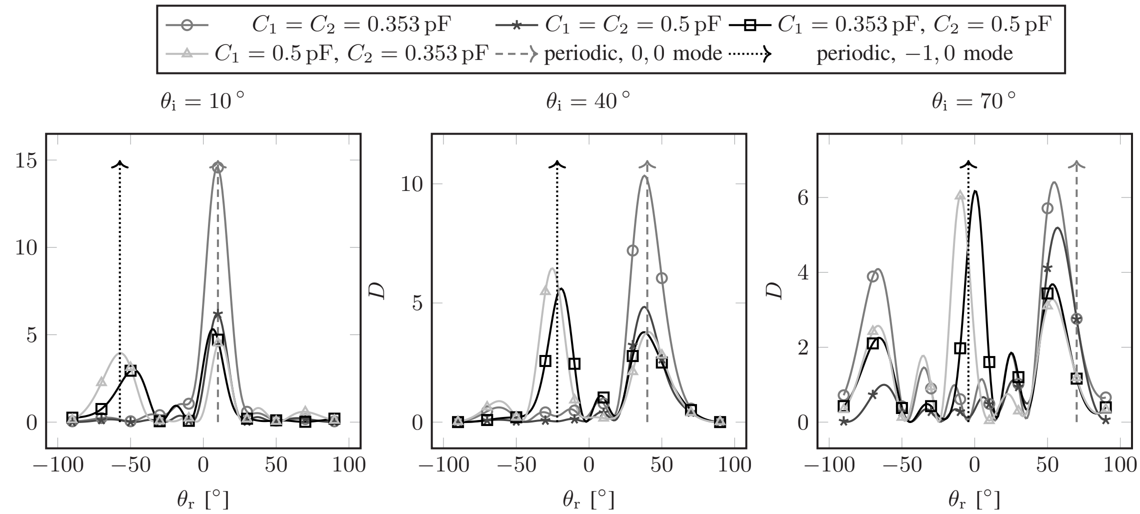

Fig. 8. Directivity of the finite RIS structure, $\phi_\mathrm{i} = 0\,°$, $f = 4.7\,\mathrm{GHz}$. Arrows are normalized to match D.

[8] M. H. Jwair and T. A. Elwi, "Metasurface antenna circuitry for 5G communication networks," *Infocommunications Journal*, vol. 15, no. 2, pp. 2–7, 2023, DOI: 10.36244/ICJ.2023.2.1.

[10] V. Degli-Esposti, E. M. Vitucci, M. D. Renzo, and S. A. Tretyakov, "Reradiation and scattering from a reconfigurable intelligent surface: A general macroscopic model," *IEEE Transactions on Antennas and Propagation*, vol. 70, no. 10, pp. 8691–8706, Oct. 2022, DOI: 10.1109/TAP.2022.3149660.

[11] E. Björnson, H. Wymeersch, B. Matthiesen, P. Popovski, L. Sanguinetti, and E. de Carvalho, "Reconfigurable intelligent surfaces: A signal processing perspective with wireless applications," *IEEE Signal Processing Magazine*, vol. 39, no. 2, pp. 135–158, Mar. 2022, DOI: 10.1109/MSP.2021.3130549.

[12] A. Díaz-Rubio, V. S. Asadchy, A. Elsakka, and S. A. Tretyakov, "From the generalized reflection law to the realization of perfect anomalous reflectors," *Science Advances*, vol. 3, no. 8, Aug. 2017, DOI: 10.1126/SCIADV.1602714.

[13] G. Xu, V. G. Ataloglou, S. V. Hum, and G. V. Eleftheriades, "Extreme beam-forming with impedance metasurfaces featuring embedded sources and auxiliary surface wave optimization," *IEEE Access*, vol. 10, pp. 28 670–28 684, 2022, DOI: 10.1109/ACCESS.2022.3157291.

[14] V. G. Ataloglou, T. Qiu, and G. V. Eleftheriades, "Design of dual-polarization reflective impedance metasurfaces for 3D beam-shaping," in *2024 IEEE International Symposium on Antennas and Propagation and INC/USNC-URSI Radio Science Meeting*. Firenze, Italy: IEEE, Jul. 2024, pp. 1501–1502, DOI: 10.1109/AP-S/INC-USNC-URSI52054.2024.10686554.

[15] B. T. Csathó, Z. Badics, J. Pávó, and B. P. Horváth, "Accelerated 3-D analysis of metasurfaces for RIS applications by characteristic cell functions," *IEEE Transactions on Magnetics*, vol. 60, no. 12, pp. 1–4, Dec. 2024, DOI: 10.1109/TMAG.2024.3480354.

[16] Y. Liu and C. D. Sarris, "Efficient propagation modeling for communication channels with reconfigurable intelligent surfaces," *IEEE Antennas and Wireless Propagation Letters*, vol. 21, no. 10, pp. 2120–2124, Oct. 2022, DOI: 10.1109/LAWP.2022.3192269.

[17] Özlem Tuğfe Demir and E. Björnson, "Wideband channel capacity maximization with beyond diagonal RIS reflection matrices," *IEEE Wireless Communications Letters*, vol. 13, no. 10, pp. 2687–2691, Oct. 2024, DOI: 10.1109/LWC.2024.3439489.

[18] A. Abrardo, A. Toccafondi, and M. D. Renzo, "Design of reconfigurable intelligent surfaces by using S-parameter multiport network theory — Optimization and full-wave validation," *IEEE Transactions on Wireless Communications*, vol. 23, no. 11, pp. 17 084–17 102, Nov. 2024, DOI: 10.1109/TWC.2024.3450722.

[19] A. Diaz-Rubio and S. A. Tretyakov, "Macroscopic modeling of anomalously reflecting metasurfaces: Angular response and far-field scattering," *IEEE Transactions on Antennas and Propagation*, vol. 69, no. 10, pp. 6560–6571, Oct. 2021, DOI: 10.1109/TAP.2021.3076267.

[20] A. K. Bhattacharyya, *Phased Array Antennas: Floquet Analysis, Synthesis, BFNs, and Active Array Systems*. Hoboken, NJ, USA: Wiley, 2006.

[21] L. B. Felsen and N. Marcuvitz, *Radiation and Scattering of Waves*. Hoboken, NJ, USA: Wiley, 2003.

[22] C. A. Balanis, *Advanced Engineering Electromagnetics*, 2nd ed. Hoboken, NJ, USA: Wiley, 2013.

[23] ANSYS, Inc., ANSYS® Academic Research High-Frequency Structure Simulator, Release 21.2, *HFSS Help*, Jul. 2021.

[24] C. Yepes, M. Faenzi, S. Maci, and E. Martini, "Perfect non-specular reflection with polarization control by using a locally passive metasurface sheet on a grounded dielectric slab," *Applied Physics Letters*, vol. 118, no. 23, Jun. 2021, DOI: 10.1063/5.0048970.

Botond Tamás Csathó is currently pursuing his Ph.D. at the Budapest University of Technology and Economics. He received his M.Sc. in 2021 from the same institute. His research interests include electromagnetic modeling of metasurfaces and signal processing for multiple antenna communications.

Bálint Péter Horváth received his M.Sc. 2013 and Ph.D. 2018 degrees in Electrical Engineering from the Budapest University of Technology and Economics, where he is currently a senior lecturer at the Department of Broadband Infocommunications and Electromagnetic Theory. His research interests include signal processing in communications systems, software defined radio, electromagnetic simulations and computational model validation of wireless devices.